RSC Advances

ROYAL SOCIETY OF CHEMISTRY

www.rsc.org/advances

Enhanced high rate performance of $Li[Li_{0.17}Ni_{0.2}Co_{0.05}Mn_{0.58-x}Al_x]O_{2-0.5x}$ cathode material for lithium-ion batteries

Y. L. Wang, X. Huang, F. Li, J. S. Cao, and S. H. Ye*

Institute of New Energy Material Chemistry, Tianjin Key Laboratory of Metal and Molecule Based Material Chemistry, Collaborative Innovation Center of Chemical Science and Engineering (Tianjin), Nankai University, Tianjin 300071, China. Fax:/Tel: +86-22-23500876, E-mail: yeshihai@nankai.edu.cn

Graphical Abstract

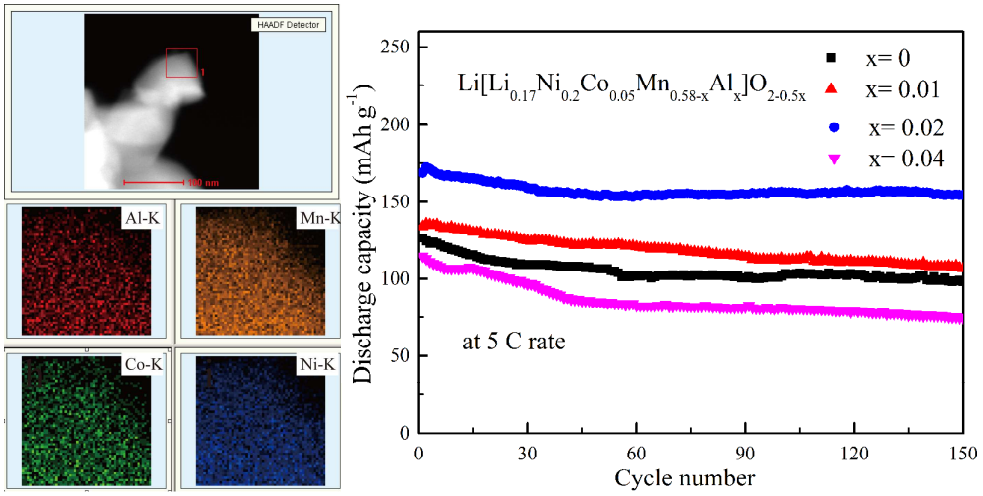

Cite this: DOI: 10.1039/c0xx00000x

www.rsc.org/xxxxxx

Paper

Enhanced high rate performance of $Li[Li_{0.17}Ni_{0.2}Co_{0.05}Mn_{0.58-x}Al_x]O_{2-0.5x}$ cathode material for lithium-ion batteries

Y. L. Wang, X. Huang, F. Li, J. S. Cao and S. H. Ye*

Received (in XXX, XXX) Xth XXXXXXXXX 20XX, Accepted Xth XXXXXXXXX 20XX

DOI: 10.1039/b000000x

The pristine $Li[Li_{0.17}Ni_{0.2}Co_{0.05}Mn_{0.58}]O_2$ (LNCM) and $Li[Li_{0.17}Ni_{0.2}Co_{0.05}Mn_{0.58-x}Al_x]O_{2-0.5x}$ (x=0.01, 0.02 and 0.04) (LNCMA) as Li-rich cathode materials for lithium ion batteries are synthesized via a sol-gel route. The inductively coupled plasma atomic emission spectrometer (ICP-AES), X-ray diffraction (XRD), scanning electron microscope (SEM) and transmission electron microscope (TEM) are used to investigate the composition, structure and morphology of LNCM and LNCMA samples. The homogeneous dispersion of Al element in the LNCMA samples is confirmed via the energy dispersive spectroscopic (EDS) mapping. Compared with LNCM, the larger crystal cell volume of LNCMA is verified by XRD and TEM analysis. The blue shift of O1s and Mn2p peaks in the A2 sample is observed via XPS, demonstrating the partial substitution of Al^{3+} for Mn^{4+} ions. The electrochemical properties are examined by means of cyclic voltammetry and charge/discharge tests. In general, the Al-substituted samples exhibit a better electrochemical performance. Especially for the A2 sample, it presents enhanced initial discharge capacity of ~300 mAh g^{-1}, accompanied with the better initial coulombic efficiency of 90.9%. For 5 C rate, the A2 sample delivers a higher discharge capacity of 168.9 mAh g^{-1} in the initial cycle and 156.5 mAh g^{-1} after 150 cycles, while for the pristine sample it is 126.5 and 98.8 mAh g^{-1}, respectively. The excellent electrochemical performance of Al-substituted samples could be ascribed to the enlarged cell volume and improved strutural stability resulting from the partial Al substitution.

Introduction

Fossil fuels such as coal and oil as non-renewable resources are facing the energy depletion problem.[1, 2] Exploitation of new energy has been abstracting more and more attention.[3-5] Among them, solar, wind, tidal and other new energy greatly depend on time and space.[6, 7] Thus, Lithium ion batteries (LIBs) as a portable energy storage and conversion device have been widely applied in many fields such as consumer electronics products and electric vehicles (EVs).[8] Up to now, commercial cathode materials for LIBs have been facing the challenge from the low theoretical specific capacity and the low high-rate performance.[9-11] The lithium-rich layered materials seem to be very promising candidates as cathode because of their high discharge capacity (250 - 300 mAh g^{-1}).[12-14] However, these materials have to overcome many problems such as the low initial coulombic efficiency and the low rate capability caused by the change of surface structure and poor electrical conductivity.[13, 15, 16] Previous studies suggest that Jahn-Teller distortion and dissolution of manganese into the electrolyte solution leads to the lithium layered oxide capacity degradation,[17-19] and Mn^{3+} ions take major charge in the poor cycling performance because they can convert into Mn^{2+} or Mn^{4+} during a disproportional reaction.[13, 20, 21] Great efforts have been made to search for effective methods to improve the electrochemical properties of this interesting cathode material, especially on its cycling stability and rate capability, by means of synthesis methods, [22] doping,[11, 17, 19, 23-30] and surface coating.[31-36] The former can increase the average oxidation state of Mn in the bulk of Li-rich layered oxides while the latter can decrease the contacting area with electrolyte. Among the introduced elements, Al has attracted much attention because it is abundant, nontoxic, cheaper and lighter than transition metal elements. More importantly, $LiAlO_2$ as a well-known lithium ion conductor can enhance the ionic conductivity of the LNCM. Moreover, Al^{3+} ions in the host structure may strengthen the stability of the crystal structure by introducing some Al–O bonds. Furthermore, the stronger Al-O bonds may suppress the oxygen vacancy diffusion so that the irreversible discharge capacity is decreased.[11, 17, 30, 37, 38]

In this work, the pristine $Li[Li_{0.17}Ni_{0.2}Co_{0.05}Mn_{0.58}Al]O_2$ and $Li[Li_{0.17}Ni_{0.2}Co_{0.05}Mn_{0.58-x}Al_x]O_{2-0.5x}$ (x=0.01, 0.02 and 0.04) are prepared by a sol-gel method. The impact of the introduced Al^{3+} ions on the structure and electrochemical properties of Li-rich layered oxides are researched. The A2 sample shows better

cycling stability and higher rate performance compared with the pristine sample.

Experimental

Preparation of $Li[Li_{0.17}Ni_{0.2}Co_{0.05}Mn_{0.58-x}Al_x]O_{2-0.5x}$ (x=0, 0.01, 0.02, 0.04)

All chemical reagents were purchased from Tianjin Guangfu Co. Ltd. in China and not further purified. The $Li[Li_{0.17}Ni_{0.2}Co_{0.05}Mn_{0.58-x}Al_x]O_{2-0.5x}$ (x=0, 0.01, 0.02, 0.04) named A0, A1, A2 and A4 sample, were prepared according to previous method.[29] Firstly, a mixture of $Ni(CH_3COO)_2{\cdot}4H_2O$ (1.24 g, AR), $Co(CH_3COO)_2{\cdot}4H_2O$ (0.31 g, AR) and $Li(CH_3COO){\cdot}2H_2O$ (3.21 g. AR) were dissolved in distilled water (250 mL). Under stirred, the stoichiometric $Mn(CH_3COO)_2{\cdot}4H_2O$ (AR) and $Al(NO_3)_3{\cdot}9H_2O$ (AR) were added in the above solution to obtain mixed solution. For A0, A1, A2 and A4 samples, the addition amount of $Mn(CH_3COO)_2{\cdot}4H_2O$ is 3.5740, 3.4940, 3.4326 and 3.3100 g, respectively. Correspondingly, the amount of $Al(NO_3)_3{\cdot}9H_2O$ additive is 0, 0.0938, 0.1876 and 0.3755 g, respectively. Finally, citric acid solution (23.095 g in 100 ml distilled water) was dripped slowly into the solution. The pH of the solution is controlled at 9−11 by ammonia solution. The light green solution was stirred vigorously to evaporate at 80ºC until gel occurred. The gel was preheated at 450°C for 5 h. After grinded hard for 30 mins, the powder materials were calcined in muffle furnace at 850ºC for 10 h. The whole thermal treatment was performed under air atmosphere.

Characterization of materials

The structure of the samples was confirmed by X-ray diffraction (Rigaku Rint 1000) with a range of 2θ from 10° to 80° at a rate of 2° min^{-1}. Rietveld refinement was performed using the program Jade 6.0. The composition and morphology were characterized by ICP-AES (IRIS Intrepid IIXSP), SEM (Hitachi, S-4800) and TEM (FEI Tecnai F20) equipped with EDS. X-ray photoelectron spectroscopy (XPS, PHI 5000 Versa probe) and differential scanning calorimetry (DSC, Mettler Toledo) were used to investigate surface state and thermal stability of the materials.

Electrochemical measurements

The as-prepared samples, the acetylene black and polytetrafluoroethylene (PTFE) were mixed at a weight ratio of 75:15:10 to prepare the working electrode. Metallic lithium served as both of the counter electrode and reference electrode. The electrolyte is $LiPF_6$ (1 M) in a mixture of ethylene carbonate (EC) and dimethyl carbonate (DMC) with a volume ratio of 3:7. The chronoamperometry method was employed to measure the electrochemical capacity of the cathodes at 25°C using LAND-CT2001A instrument with a charge-discharge current density of 0.1 C rate (30 mA g^{-1}). The high rate capability was also conducted at different current densities. The cut-off voltage window for charge and discharge processes was set at 4.8 V and 2.0 V, respectively.

Results and discussion

XRD patterns of $Li[Li_{0.17}Ni_{0.2}Co_{0.05}\ Mn_{0.58-x}Al_x]O_{2-0.5x}$ (x=0, 0.01, 0.02 and 0.04) are shown in Fig.1. All the peaks from 2θ = 10–80º are identified as a single-phase R-3m space group, including the super lattice peaks found between 2θ = 22-30º,[29] characteristic of a Li_2MnO_3-type integrated phase. In the Al-substituted LNCM sample, no peaks of impurities can be observed indicating that the Al^{3+} could be considered to incorporate into all the octahedral sites of Li_2MnO_3 layer.[37, 38]

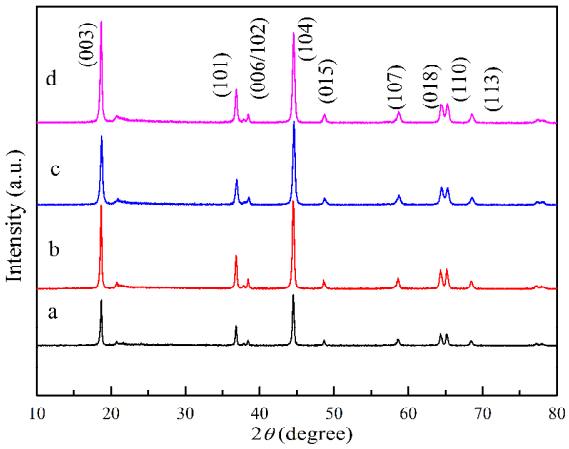

Fig. 1 X-Ray diffraction spectra of $Li[Li_{0.17}Ni_{0.2}Co_{0.05}\ Mn_{0.58-x}Al_x]O_{2-0.5x}$ powders. x = 0 (a), x = 0.01 (b), x = 0.02 (c) and x = 0.04 (d)

The lattice constants obtained from the Rietveld refinement on the XRD data are listed in Table 1. The data show that when substituted with a small amount of Al element there is almost no change in the *a*-lattice parameter direction but a slight increase in the c-lattice parameter as well as the cell volume. It is attributed to the larger ionic radius of Al^{3+}(r (Al^{3+}) = 67.5 pm) compared with the ionic radius of Mn^{4+}(r (Mn^{4+}) = 67 pm).[30, 39] The increase of the cell volume is beneficial to the faster Li^+ diffusion due to the decrease of the activation energy of Li hopping.[40] The *c*/*a* ratio is an indication of the hexagonal setting. The high *c*/*a* ratio (>4.96) implies a well-ordered layered structure.[17] Thus it can be concluded that Al substitution for Mn does not strongly impact the bulk crystal structure.

Table 1 Rietveld refinement results of XRD data for $Li[Li_{0.17}Ni_{0.2}Co_{0.05}Mn_{0.58-x}Al_x]O_{2-0.5x}$ (x=0, 0.01, 0.02 and 0.04)

Sample	*a* (Å)	Error (*10^{-3})	*c* (Å)	Error (*10^{-3})	*c*/*a*	Cell volume (Å^3)
x=0	2.855	2.343	14.147	9.256	4.96	99.86
x=0.01	2.856	0.31	14.188	3.177	4.97	100.22
x=0.02	2.856	1.812	14.191	5.551	4.97	100.24
x=0.04	2.856	0.745	14.227	4.574	4.98	100.50

Typical powder morphologies and components of the sample A0, A1, A2 and A4 studied by SEM and EDS are shown in Fig.2. SEM images exhibit all the samples have an average size of about 100-200 nm. The LNCMA particles show uniform particle size. The corresponding EDS analysis of all the samples are shown in Fig. 2(e-h), respectively. Among those of three Al-substituted samples, Al element can be observed, of which the peak intensity increases with the increasing of Al content, verifying the actual presence of Al in the LNCMA samples.

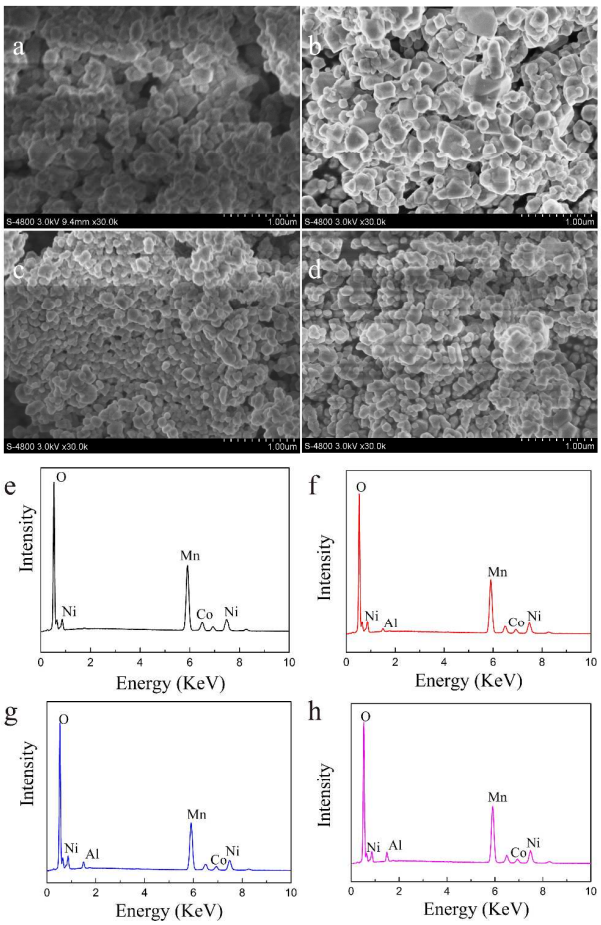

Fig.2 SEM images of $Li[Li_{0.17}Ni_{0.2}Co_{0.05}Mn_{0.58-x}Al_x]O_{2-0.5x}$ samples with x = 0 (a), 0.01 (b), 0.02 (c) and 0.04 (d). The EDS analysis for samples with x = 0 (e), 0.01 (f), 0.02 (g) and 0.04 (h).

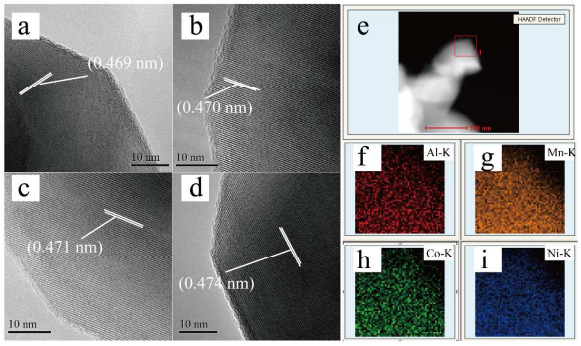

Fig.3 HRTEM images of the $Li[Li_{0.17}Ni_{0.2}Co_{0.05}Mn_{0.58-x}Al_x]O_{2-0.5x}$ samples with x = 0 (a), 0.01 (b), 0.02 (c) and 0.04 (d). HAADF image (e) and the corresponding elemental maps of Al (f), Mn (g), Co (h) and Ni (i) element in the $Li[Li_{0.17}Ni_{0.2}Co_{0.05}Mn_{0.58-x}Al_x]O_{2-0.5x}$ (x = 0.02) sample

To further understand the morphology and microstructure details of the LNCM and LNCMA composites, the high-resolution transmission electron microscopy (HRTEM), high-angle annular dark-field (HAADF) and the corresponding elemental mapping are performed, shown in Fig.3. For the pristine and Al-substituted samples, a continuous interference fringe spacing can be observed, which related to lattice plane (003). The interplanar spacing is increasing from 0.469 to 0.474 nm with increase of x value, indicating the cell volume is expanded by the introduction of Al-element. It is in agreement with the XRD analysis. HAADF image and the corresponding elemental maps of the A2 sample are utilized to investigate distribution of Al in the structure of material, where the image intensity is directly related to area concentration. Aluminium has a homogenous distribution in the random region (square 1 in the STEM image in Fig.3e). The quantitative analysis is carried out by inductively coupled plasma emission spectrometer (ICP-AES). For the as-prepared A0, A1, A2 and A4 samples, the determined element content of Li, Ni, Co, Mn and Al is very closed to the raw material ratio as designed, shown in Table 2.

Table. 2 The element content of $Li[Li_{0.17}Ni_{0.2}Co_{0.05}Mn_{0.58-x}Al_x]O_{2-0.5x}$ samples with x = 0, 0.01, 0.02 and 0.04 performed by ICP-AES

Samples		Li	Ni	Co	Mn	Al
x = 0	Designed	1.17	0.2	0.05	0.58	
	As-prepared	1.176	0.192	0.049	0.583	
x = 0.01	Designed	1.17	0.20	0.05	0.57	0.01
	As-prepared	1.170	0.210	0.049	0.569	0.011
x = 0.02	Designed	1.17	0.2	0.05	0.56	0.02
	As-prepared	1.177	0.195	0.052	0.553	0.024
x = 0.04	Designed	1.17	0.20	0.05	0.54	0.04
	As-prepared	1.171	0.197	0.049	0.539	0.042

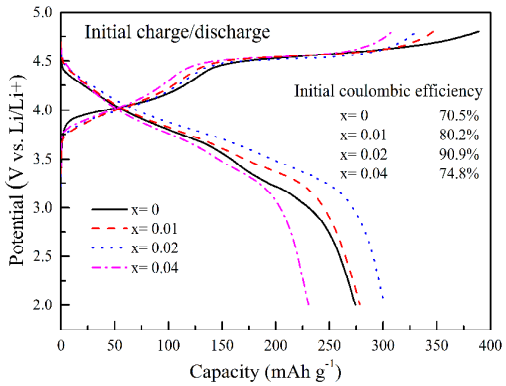

Fig.4 The charge–discharge curves of $Li[Li_{0.17}Ni_{0.2}Co_{0.05}Mn_{0.58-x}Al_x]O_{2-0.5x}$ composites with x = 0, 0.01, 0.02 and 0.04 at a rate of 0.1 C.

Fig.4 shows the initial charge/discharge curves of all the samples during cycling at 0.1 C rate (30 mA g^{-1}). The initial charge capacities of the A0, A1, A2 and A4 samples are 389.0, 346.9, 349.4 and 308.2 mAh g^{-1}, respectively. The charge curves are composed of a slope at potential region from 3.7 V to 4.5 V and a potential plateau from 4.5 to 4.8 V. For all the samples, the charge capacity located at the slope are similar (~ 150 mAh g^{-1}), which should be related to the extraction of Li^+ ions from the layered structure as well as the oxidation of Ni^{2+} to Ni^{4+}.[13, 39] Compared with the pristine samples, the Al-substituted samples exhibit fewer charge capacity at the potential plateau of 4.5 - 4.8 V, which is attributed to the irreversible extraction of Li^+ ions as Li_2O form or the irreversible oxidation of O^{2-} ions.[13, 41, 42] It means the introduction of Al element supresses the irreversible process. The initial coulombic efficiency for the pristine sample is only 70.5% while the initial coulombic efficiency for all the Al-substituted samples (x = 0.01, 0.02 and 0.04) reaches up to 80.2%, 88.8% and 74.8%, respectively. Among all of them the Al-substituted with x = 0.02 sample has the maximum initial discharge capacity (310.2 mAh g^{-1}). The sample with x=0.04

presents lower charge and discharge capacity compared with the other samples, may be due to more Al^{3+} substitution of Mn^{4+} could restrain Li_2MnO_3 layer activation in the initial charge process although the structure is more stable. And another explanation is that Al^{3+} is electrochemical inert. The few new layer structure composed of Al^{3+} substitution cannot devote charge/discharge capacity.

Cyclic voltammetry (CV) measurements were operated to get information about different redox processes at a scan rate of 0.1 mV s^{-1} between 2.0 and 4.8 V (vs. Li/Li^+). CVs of the initial three cycles are shown in Fig.5. In the case of the pristine sample in the initial cycle, there are two oxidation peaks located at 4.01 and 4.69 V and the former is related to the reversible extraction of Li^+ ions from the layered structure while the latter to the irreversible extraction of Li^+ ions as Li_2O form, respectively.[13] There are three reduction peaks located at 4.23, 3.69 and 3.35 V, attributed to the reduction of Co^{4+}, Ni^{4+} and Mn^{4+} ions, respectively.[43, 44] In the second cycle, the sharp oxidation peak at 4.69 V decreases to a weak and wide peak and the latter should be attributed to the oxidation of Co^{3+} ions. The oxidation peak at 4.01 V shifts to 3.92 V, related to the modification of layered structure in the initial oxidation process.[13] The reduction peak at 3.35 V shifts to 3.25 V and its peak intensity increase, attributed to the reduction of Mn^{4+} ions. For the Al-substituted samples, there is no obvious difference between their oxidation processes during the three cycles. In the initial reduction process, all Al-substituted samples exhibit a stronger reduction peak at 3.32 V than that of the pristine sample. The intensity of the peak in 3 cycles is more similar for the Al-substituted samples than that of the pristine sample, indicating the more stable reduction process of the Al-substituted samples. It should be attributed to the improvement of structural stability via the partial substitution of Mn^{4+} by Al^{3+}.

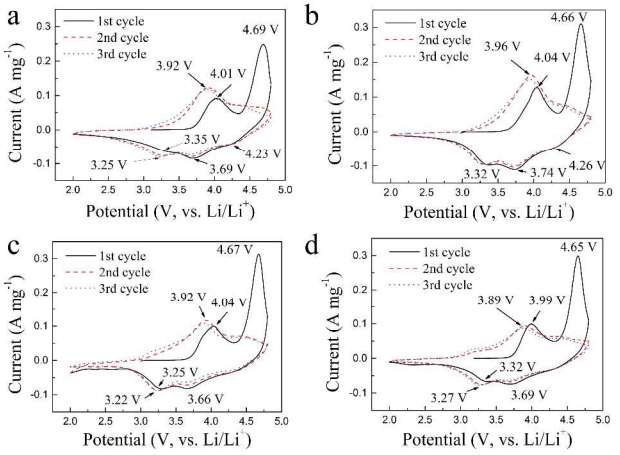

Fig.5 Cyclic voltammograms of the $Li[Li_{0.17}Ni_{0.2}Co_{0.05}Mn_{0.58-x}Al_x]O_{2-0.5x}$ cells in the 2.0 - 4.8 V range at the scan rate of 1 mV s^{-1}: (a) x = 0, (b) x = 0.01, (c)x = 0.02, and (d) x = 0.04

The cycling performances of sample A0, A1, A2 and A4 at room temperature are shown in Fig.6. At 0.1 C (Fig. 6a), the initial discharge capacity of the A0 samples is 274.1 mAh g^{-1}. It remains 236.4 mAh g^{-1} after 70 cycles. The capacity retention ratio is about 86.2%. A2 sample exhibits a higher initial discharge capacity of 301.2 mAh g^{-1} and a little better capacity retention ratio of 88.9%. A1 sample presents the similar initial discharge capacity and a little better capacity retention ratio. For the A4 sample, the initial discharge capacity is lower (236.9 mAh g^{-1}), but the capacity retention ratio is much higher (96.1%). The results indicate that all Al-substituted samples present a better cyclic stability. It could be due to that Al-substitution stabilizes the crystal structure and supresses the LNCMA structure change. It is noted that A2 sample delivers an extra capacity of ~ 30 mAh g^{-1} during cycles.

The high rate performance of LNCM and LNCMA are shown in Fig.6b (1 C) and Fig.6c (5 C). For 1 C rate, the initial discharge capacities of the sample A0, A1, A2 and A4 are 152.9 196.0, 229.0 and 140.0 mAh g^{-1}, respectively. After 70 cycles, the discharge capacities of the samples retains at 136.8, 178.6, 204.5 and 109.9 mAh g^{-1}, respectively. The corresponding capacity retention ratio is 89.5%, 91.1%, 89.3% and 78.5%. A1 and A2 samples can deliver a much higher cyclic capacity. For 5 C rate, the cyclic discharge capacity of all samples decreases drastically. Even so, the A2 sample delivers a higher discharge capacity of 168.9 mAh g^{-1} in the initial cycle and 156.5 mAh g^{-1} after 150 cycles, while for the pristine sample it is 126.5 and 98.8 mAh g^{-1}, respectively. It means that the high rate performance of LNCM can be improved via Al element substitution, as also verified by the various rates test. Fig.6d shows the discharge capacity at various rates for 10 cycles. At varied charge/discharge current densities the A2 sample has stable discharge capacity. It means that the A2 sample can endure great changes of current densities and still retain high stability upon cycling, showing the stronger structural stability. Specially, A4 sample presents the lowest cyclic capacity at above rates among all samples, however, it still exhibits superior cyclic stability at 0.1 C rate and better high rate performance than those of A0 sample. The higher current density is, the less the capacity difference between of A4 and A0 sample is. It means the substitution of Al^{3+} for partial Mn^{4+} is beneficial for improving the structural stability and high rate performance of LNCM oxide, due to the Al^{3+} electrochemical inert and larger Li ion diffusion channel.

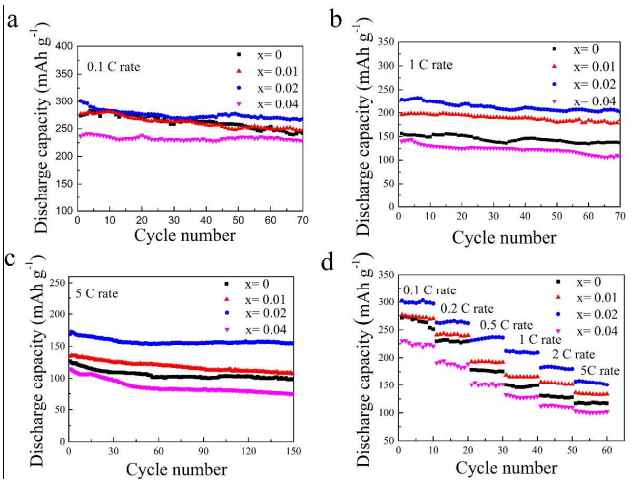

Fig.6 The cycle performance of $Li[Li_{0.17}Ni_{0.2}Co_{0.05}Mn_{0.58-x}Al_x]O_{2-0.5x}$ cells at: 0.1 C , 1 C, 5 C and various rates in the voltage range of 2.0–4.8 V at room temperature: (a) x = 0, (b) x = 0.01, (c) x = 0.02, and (d) x = 0.04

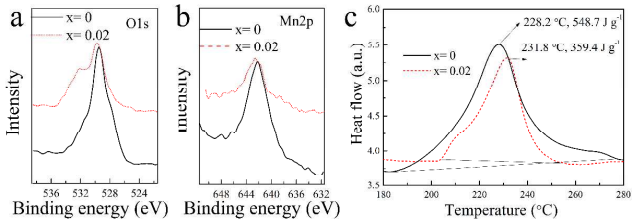

Fig.7 The X-ray photoelectron spectra of the $Li[Li_{0.17}Ni_{0.2}Co_{0.05}Mn_{0.58-x}Al_x]O_{2-0.5x}$ (x = 0, 0.02) (a and b) and DSC profiles of the $Li[Li_{0.17}Ni_{0.2}Co_{0.05}Mn_{0.58-x}Al_x]O_{2-0.5x}$ (x = 0, 0.02) after charging to 4.8 V (vs. Li/Li^+) in the first cycle (c)

Fig. 7a and b shows the binding energy of O1s and Mn2p in the A0 and A2 samples, measured by XPS. The O1s peak at 529.5 eV of the pristine sample is in accordance with the lattice oxygen of the Li-rich layered oxides.[44] It shifts to 532.14 eV in the A2 sample, as well as the blue shift of Mn2p peak from 642.1 to 642.7 eV. The increase of binding energy of O1s can be explained as the higher binding energy of O1s in Al_2O_3 lattice (532.7 eV) than that in MnO_2 lattice (529.5 eV).[45, 46]The blue shift of Mn2p is attributed to the charge compensation resulting from the partial substitution of Al^{3+} for Mn^{4+} ions in the layered oxide. It implies that in the modified samples the partial Mn^{4+} ions are substituted by Al^+ ions, which resulting in the blue shift of O1s peak and Mn2p peak. Fig.7c shows the DSC curves of the samples A0 and A2 after charged to 4.8 V (vs. Li/Li^+) in the first cycle. The heat associated with the exothermic peak is 548.7 and 359.4 J g^{-1} for the sample A0 and A2, respectively. Evidently, the heat released by sample A2 is lower than that of the A0, as well as the exothermic temperature, indicating the thermal stability of A2 sample is improved via the Al substitution. It can be explained that the Al–O bond (512 kJ mol^{-1}) is much higher compared with the Mn–O bond (402 kJ mol^{-1}). The stronger bonding induced by incorporation of Al–O in the host structure can improve the structural stability of Al-substituted samples. Therefore, the excellent electrochemical performance can be attributed to the larger cell volume, more stable structure and the higher thermal stability caused by the Al substitution.

Conclusions

The $Li[Li_{0.17}Ni_{0.2}Co_{0.05}Mn_{0.58-x}Al_x]O_{2-0.5x}$ (x= 0, 0.01, 0.02, 0.04) materials are successfully synthesized via a sol-gel and subsequent calcination. Al substitution exerts no great influence on the bulk phase and morphology of Li-rich layered oxide. Via the substitution of Al, the cell volume is enlarged and the core levels of O1s and Mn2p are strengthened for the sample A2. The $Li[Li_{0.17}Ni_{0.2}Co_{0.05}Mn_{0.58-x}Al_x]O_{2-0.5x}$ (x=0.02) electrode delivers much higher discharge capacity as well as cycling capability at 0.1 C and at higher current density. It should be ascribed to the enlarged cell volume, more stable structure and the higher thermal stability via the partial substitution of Mn^{4+} by Al^{3+} ions. This substitution technique offers an approach for the modification of Li-rich layered oxides as lithium ion cathode.

Acknowledgements

The Financial Supports from NSFC (21273119), TSFC (15JCYBJC21500), 973 Program (2015CB251100), and the MOE Innovation Team (IRT13022) of China are gratefully acknowledged.

Notes and references

Institute of New Energy Material Chemistry, Tianjin Key Laboratory of Metal and Molecule Based Material Chemistry, Chemistry College, Nankai University, Tianjin 300071, China. Tel: +86-22-23502604; E-mail: yeshihai@nankai.edu.cn

1. E. Tzimas and S. D. Peteves, *Energy*, 2005, **30**, 2672.
2. R. Ramanathan, *Energy*, 2005, **30**, 2831.
3. H. Lund, *Energy*, 2005, **30**, 2402.
4. T. Fanning, C. Jones and M. Munday, *Energy*, 2014, **76**, 958.
5. P. P. Edwards, V. L. Kuznetsov, W. I. F. David and N. P. Brandon, *Energy Policy*, 2008, **36**, 4356.
6. P. de Almeida and P. D. Silva, *Energy Policy*, 2009, **37**, 1267.
7. P. Tavner, *Energy Policy*, 2008, **36**, 4397.
8. M. Armand and J. M. Tarascon, *Nature*, 2008, **451**, 652.
9. J. B. Goodenough, *J. Power Sources*, 2007, **174**, 996.
10. X.-P. Gao and H.-X. Yang, *Energy Environ. Sci.*, 2010, **3**, 174.
11. K. Arbi, S. Mandal, J. M. Rojo and J. Sanz, *Chem. Mater.*, 2002, **14**, 1091.
12. Y.-K. Sun, S.-T. Myung, B.-C. Park, J. Prakash, I. Belharouak and K. Amine, *Nature Materials*, 2009, **8**, 320.
13. A. R. Armstrong, M. Holzapfel, P. Novak, C. S. Johnson, S.-H. Kang, M. M. Thackeray and P. G. Bruce, *J. Am. Chem. Soc.*, 2006, **128**, 8694.
14. J. Yan, X. Liu and B. Li, *Rsc Advances*, 2014, **4**, 63268.
15. K. Chen, Y. Shen, J. Jiang, Y. Zhang, Y. Lin and C.-W. Nan, *J. Mater. Chem. A*, 2014, **2**, 13332.
16. H. B. Lin, Y. M. Zhang, H. B. Rong, S. W. Mai, J. N. Hu, Y. H. Liao, L. D. Xing, M. Q. Xu, X. P. Li and W. S. Li, *J. Mater. Chem. A*, 2014, **2**, 11987.
17. C. J. Jafta, K. I. Ozoemena, M. K. Mathe and W. D. Roos, *Electrochim. Acta*, 2012, **85**, 411.
18. F. Zhou, X. Zhao and J. R. Dahn, *J. Electrochem. Soc.*, 2009, **156**, A343.
19. F. Zhou, X. Zhao, C. Goodbrake, J. Jiang and J. R. Dahn, *J. Electrochem. Soc.*, 2009, **156**, A796.
20. C. Y. Ouyang, X. M. Zeng, Z. Sljivancanin and A. Baldereschi, *J. Phys. Chem. C*, 2010, **114**, 4756.
21. T. Thompson, J. Wolfenstine, J. L. Allen, M. Johannes, A. Huq, I. N. David and J. Sakamoto, *J. Mater. Chem. A*, 2014, **2**, 13431.
22. J.-B. Liu, L.-B. Kong, M. Xing, M. Shi, Y.-C. Luo and L. Kang, *Rsc Advances*, 2015, **5**, 3352.
23. L. F. Jiao, M. Zhang, H. T. Yuan, M. Zhao, J. Guo, W. Wang, X. D. Zhou and Y. M. Wang, *J. Power Sources*, 2007, **167**, 178.
24. D. Liu, Y. Lu and J. B. Goodenough, *J. Electrochem. Soc.*, 2010, **157**, A1269.
25. Z. Q. Deng and A. Manthiram, *J. Phys. Chem. C*, 2011, **115**, 7097.
26. S. H. Kang and K. Amine, *J. Power Sources*, 2005, **146**, 654.
27. S.-W. Cho, G.-O. Kim and K.-S. Ryu, *Solid State Ionics*, 2012, **206**, 84.
28. S. B. Park, W. S. Eom, W. I. Cho and H. Jang, *J. Power Sources*, 2006, **159**, 679.
29. H. Z. Zhang, Q. Q. Qiao, G. R. Li and X. P. Gao, *J. Mater. Chem. A*, 2014, **2**, 7454.

30. Z. Tang, X. Li and Z. Wang, *Ionics*, 2013, **19**, 1495.
31. G. R. Li, X. Feng, Y. Ding, S. H. Ye and X. P. Gao, *Electrochim. Acta*, 2012, **78**, 308.
32. Q. Q. Qiao, H. Z. Zhang, G. R. Li, S. H. Ye, C. W. Wang and X. P. Gao, *J. Mater. Chem. A*, 2013, **1**, 5262.
33. W. Yuan, H. Z. Zhang, Q. Liu, G. R. Li and X. P. Gao, *Electrochim. Acta*, 2014, **135**, 199.
34. B. Song, C. Zhou, Y. Chen, Z. Liu, M. O. Lai, J. Xue and L. Lu, *Rsc Advances*, 2014, **4**, 44244.
35. Y. Liu, X. Huang, Q. Qiao, Y. Wang, S. Ye and X. Gao, *Electrochim. Acta*, 2014, **147**, 696.
36. X. Huang, Q. Qiao, Y. Sun, F. Li, Y. Wang and S. Ye, *J. Solid State Electrochem.*, 2015, **19**, 805.
37. Z. Li, N. A. Chernova, J. Feng, S. Upreti, F. Omenya and M. S. Whittingham, *J. Electrochem. Soc.*, 2012, **159**, A116.
38. L. Croguennec, J. Bains, J. Bréger, C. Tessier, P. Biensan, S. Levasseur and C. Delmas, *J. Electrochem. Soc.*, 2011, **158**, A664.
39. Q. Y. Wang, J. Liu, A. V. Murugan and A. Manthiram, *J. Mater. Chem.*, 2009, **19**, 4965.
40. J. D. Wilcox, E. E. Rodriguez and M. M. Doeff, *J. Electrochem. Soc.*, 2009, **156**, A1011.
41. Z. Lu and J. R. Dahn, *J. Electrochem. Soc.*, 2002, **149**, A815.
42. S. J. Shi, J. P. Tu, Y. Y. Tang, X. Y. Liu, Y. Q. Zhang, X. L. Wang and C. D. Gu, *Electrochim. Acta*, 2013, **88**, 671.
43. Z. Wang, E. Liu, C. He, C. Shi, J. Li and N. Zhao, *J. Power Sources*, 2013, **236**, 25.
44. H. Koga, L. Croguennec, M. Ménétrier, P. Mannessiez, F. Weill, C. Delmas and S. Belin, *J. Phys. Chem. C*, 2014, **118**, 5700.
45. A. F. Carley and M. W. Roberts, *An X-Ray Photoelectron Spectroscopic Study of the Interaction of Oxygen and Nitric Oxide with Aluminium*, 1978.
46. B. N. Ivanov-Emin, N. A. Nevskaya, B. E. Zaitsev and T. M. Ivanova, *Zh. Neorg. Khim.*, 1982, **27**, 3101.